Taylor & Francis
Taylor & Francis Group

RESEARCH PAPER

Check for updates

Loss of RUBCN/rubicon in adipocytes mediates the upregulation of autophagy to promote the fasting response

Tadashi Yamamuro [a,*], Shuhei Nakamura [a,b,c], Kyosuke Yanagawa [a,d], Ayaka Tokumura[a], Tsuyoshi Kawabata [a,b,e], Atsunori Fukuhara [f,g], Hirofumi Teranishi[h], Maho Hamasaki[a,b], Iichiro Shimomura[f], and Tamotsu Yoshimori [a,b,i]

aDepartment of Genetics, Graduate School of Medicine, Osaka University, Suita, Japan; bLaboratory of Intracellular Membrane Dynamics, Graduate School of Frontier Biosciences, Osaka University, Suita, Japan; cInstitute for Advanced Co-Creation Studies, Osaka University, Suita, Japan; dDepartment of Cardiovascular Medicine, Graduate School of Medicine, Osaka University, Suita, Japan; eDepartment of Stem Cell Biology, Atomic Bomb Disease Institute, Nagasaki University, Nagasaki, Japan; fDepartment of Metabolic Medicine, Graduate School of Medicine, Osaka University, Suita, Japan; gDepartment of Adipose Management, Graduate School of Medicine, Osaka University, Suita, Japan; hPharmaceutical Frontier Research Laboratories, Central Pharmaceutical Research Institute, JT Inc., Yokohama, Japan; iIntegrated Frontier Research for Medical Science Division, Institute for Open and Transdisciplinary Research Initiatives (OTRI), Osaka University, Suita, Japan

ABSTRACT

Upon fasting, adipocytes release their lipids that accumulate in the liver, thus promoting hepatic steatosis and ketone body production. However, the mechanisms underlying this process are not fully understood. In this study, we found that fasting caused a substantial decrease in the adipose levels of RUBCN/rubicon, a negative regulator of macroautophagy/autophagy, along with an increase in autophagy. Adipose-specific *rubcn*-knockout mice exhibited systemic fat loss that was not accelerated by fasting. Genetic inhibition of autophagy in adipocytes in fasted mice led to a reduction in fat loss, hepatic steatosis, and ketonemia. In terms of mechanism, autophagy decreased the levels of its substrates NCOA1/SRC-1 and NCOA2/TIF2, which are also coactivators of PPARG/PPARγ, leading to a fasting-induced reduction in the mRNA levels of adipogenic genes in adipocytes. Furthermore, RUBCN in adipocytes was degraded through the autophagy pathway, suggesting that autophagic degradation of RUBCN serves as a feedforward system for autophagy induction during fasting. Collectively, we propose that loss of adipose RUBCN promotes a metabolic response to fasting via increasing autophagic activity.

Introduction

Adipose tissue maintains metabolic homeostasis and thus prevents metabolic diseases, including dyslipidemia, fatty liver, and diabetes [1]. Adipocytes synthesize fatty acids *de novo* (lipogenesis), incorporate external fatty acids, and eventually store fatty acids as triglycerides in lipid droplets (LDs) [2]. In addition, adipocytes secrete many hormones and cytokines (called adipocytokines), thereby regulating the function of other metabolic organs such as the liver and skeletal muscle [3,4]. Adipocytes play a critical role in the metabolic response to fasting; *i.e.*, triglycerides are converted to fatty acids and glycerol in adipocytes during fasting, and the released lipids accumulate in the liver (hepatic steatosis) and are used for ketogenesis [5–7]. In adipocytes, PNPLA2/ATGL-dependent lipolysis mediates a metabolic response to fasting, but adipose-specific knockout of *Pnpla2/Atgl* does not entirely abolish this response [8], suggesting that other unknown pathways contribute to the fasting response.

Autophagy degrades unwanted proteins or organelles to maintain cellular homeostasis via metabolic turnover in neurons [9,10], the liver [11,12], muscle [13], and heart tissue [14], thereby preventing various diseases. Mitophagy, a selective form of autophagy, eliminates surplus mitochondria to regulate

adipocyte differentiation [15,16] and beige-to-white adipocyte conversion [17,18]. Lipophagy, another specific form of autophagy, degrades LDs in brown adipose tissue and the liver upon cold exposure or during chronic intermittent fasting [19,20]. Moreover, our recent study demonstrated that in adipocytes, age-dependent reduction of RUBCN/rubicon, a negative regulator of autophagy [21,22], promotes metabolic disorders by increasing the autophagic degradation of NCOA1/SRC-1 and NCOA2/TIF2 [23], which are coactivators of PPARG/PPARγ [24]. The diverse roles of autophagy in adipocytes are well characterized; however, it is not yet understood whether or how adipose autophagy participates in the metabolic response to acute fasting *in vivo*.

In this study, we found that RUBCN levels in adipocytes are dramatically reduced during fasting, and that genetic inhibition of adipose autophagy mitigates the metabolic response to fasting, including systemic fat loss, hepatic steatosis, and ketonemia. In mechanistic terms, fasting causes a reduction in the mRNA levels of adipogenic genes and a decrease in the protein levels of NCOA1 and NCOA2 (coactivators of PPARG, which is a master adipogenesis transcription factor [24]). Furthermore, we also found that RUBCN is degraded by autophagy in adipocytes during starvation. Based on these findings, we propose that loss of

---

adipose RUBCN promotes a metabolic response to fasting by upregulating autophagy.

Results

Loss of autophagy in adipocytes reduces fat loss during fasting

In a recent study, we reported that age-dependent loss of RUBCN in adipose causes systemic fat loss [23]. Because adipose RUBCN levels are also significantly reduced during fasting, we hypothesized that loss of RUBCN in adipocytes promotes fasting-induced fat loss via the upregulation of autophagy. We confirmed that fasted mice exhibited a substantial decrease in the levels of RUBCN and the autophagic substrate SQSTM1/p62 in adipose [11], and that SQSTM1 accumulated in adipose-specific *atg5* knockout mice (Figure 1A). This result suggests that autophagy in adipocytes is upregulated during fasting and is blocked in *atg5*$^{ad-/-}$ mice. Consistent with this, adipose tissue in fasted mice also exhibited a reduction in the levels of phosphorylated AKT and RPS6KB1/S6K1 (Figure 1A). This result indicates that the AKT-MTORC1 pathway, which negatively regulates autophagy [25], is inactivated. To further test our hypothesis, we examined fasting-induced weight loss of adipose-specific *rubcn*-knockout mice [23], in which autophagy is upregulated in adipocytes. In agreement with our previous report, RUBCN levels in white adipose tissue (WAT) and brown adipose tissue (BAT) were significantly reduced in *rubcn*$^{ad-/-}$ mice (Figure S1A and S1B). Relative to control mice, *rubcn*$^{ad-/-}$ mice exhibited less fasting-induced body-weight reduction (Figure 1B). Like fasted control mice, fed *rubcn*$^{ad-/-}$ mice exhibited a reduction in the weight of several types of adipose tissues, including epididymal WAT (eWAT) (Figure 1C and S2B), mesenteric WAT (mWAT) (Figure 1D and S2C), inguinal WAT (iWAT) (Figure 1E and S2D), and interscapular BAT (iBAT) (Figure 2A and S2E). Importantly, fasting did not cause additional fat loss in *rubcn*$^{ad-/-}$ mice (Figure 1C–E and S2A–E). Histological analysis revealed the same tendency in the size of white adipocytes (Figure 1F,G) and brown adipocytes (Figure S2G). These observations suggest that a fasting-induced decline in RUBCN levels promotes adipocyte size reduction. In addition, mice with adipose-specific knockout of *atg5* (Figure S1C and S1D), which is essential for autophagy, and double-knockout mice did not exhibit a systemic fat loss in fed conditions but failed to undergo a fasting-induced reduction in bodyweight (Figure 1B), adipose weight (Figure 1C–E and S2A–E), or adipocyte size (Figure 1F,G and S2G). ATG5 is essential for autophagy at the early step, while RUBCN negatively regulates autophagy at the late step [26]. Therefore, the double knockout mice exhibited autophagy deficiency in adipocytes as well as single *atg5* knockout mice [23]. The above results suggest that adipose autophagy is required for the fasting-induced fat loss. Collectively, our results indicate that loss of RUBCN mediates fasting-induced fat loss by upregulating autophagy.

Loss of autophagy in adipocytes decreases fasting-induced hepatic steatosis

We previously showed that age-dependent loss of RUBCN in adipocytes leads to hepatic steatosis by increasing autophagic activity [23]. Hepatic steatosis is also caused by the incorporation of lipids from adipose tissue during fasting [7]. Therefore, we investigated whether upregulation of autophagy in adipocytes increases the levels of triglycerides in the bloodstream or the liver during fasting. Consistent with the findings described above, fasted mice and *rubcn*$^{ad-/-}$ mice exhibited increased plasma levels of triglycerides (Figure 2A). Liver weight was similarly reduced in these knockout mice during fasting (Figure 2B and S2F), whereas fasted mice exhibited an increase in hepatic levels of triglycerides (Figure 2C). Histology revealed massive steatosis in the fasted control and *rubcn*$^{ad-/-}$ mice and abnormal hepatic lipid accumulation in fed *rubcn*$^{ad-/-}$ mice (Figure 2D). Strikingly, loss of autophagy in adipocytes attenuated an increase in plasma triglycerides (Figure 2A) and hepatic steatosis during fasting (Figure 2C–E). Our observations indicate that autophagy in adipocytes is required for fasting-induced hepatic steatosis. Because lipid accumulation is thought to be required for ketogenesis in the liver upon fasting [6], we also examined the plasma levels of ketone bodies in fasted mice. We found that loss of *atg5* in adipocytes reduced fasting-induced ketonemia (Figure 2F). Therefore, elevated autophagy in adipocytes likely contributes to ketonemia during fasting. Our knockout mouse models have highlighted the role of adipose autophagy in the metabolic response to fasting, including fat loss, hepatic steatosis, and ketonemia.

Fasting causes a substantial decrease in adipogenic gene expression: NCOA1 and NCOA2

Next, we sought to determine the mechanism by which upregulation of adipose autophagy leads to systemic fat atrophy and hepatic steatosis upon fasting. Our work showed that autophagy in adipocytes degrades NCOA1 and NCOA2 [23]. Both proteins are coactivators of PPARG, a master regulator of adipogenesis [24]. Hence, we hypothesized that increased autophagic degradation of NCOA1 and NCOA2 would lead to a decline in adipocyte function during fasting. We found that adipose tissue in fasted mice had reduced levels of mRNA for multiple adipogenic genes (Figure 3A), and the protein levels of NCOA1 and NCOA2 were also reduced (Figure 3B). This reduction in mRNA levels was attenuated by the loss of *atg5* in adipocytes (Figure 3A), suggesting that autophagy is required for a fasting-induced reduction in adipogenic gene transcription levels. Consistent with this, in 3T3-L1 adipocytes, the mRNA levels of adipogenic genes were reduced during starvation (Figure 3C–E, S3A–D), and some of these reductions were attenuated when cells were treated with bafilomycin A1, which is a lysosomal inhibitor (Figure 3C–E). Upon starvation, 3T3-L1 adipocytes exhibited a decline in NCOA1 and NCOA2 protein levels in a lysosomal activity–dependent manner (Figure 3F). Moreover, nuclear–cytoplasmic fractionation assays showed that both NCOA1 and
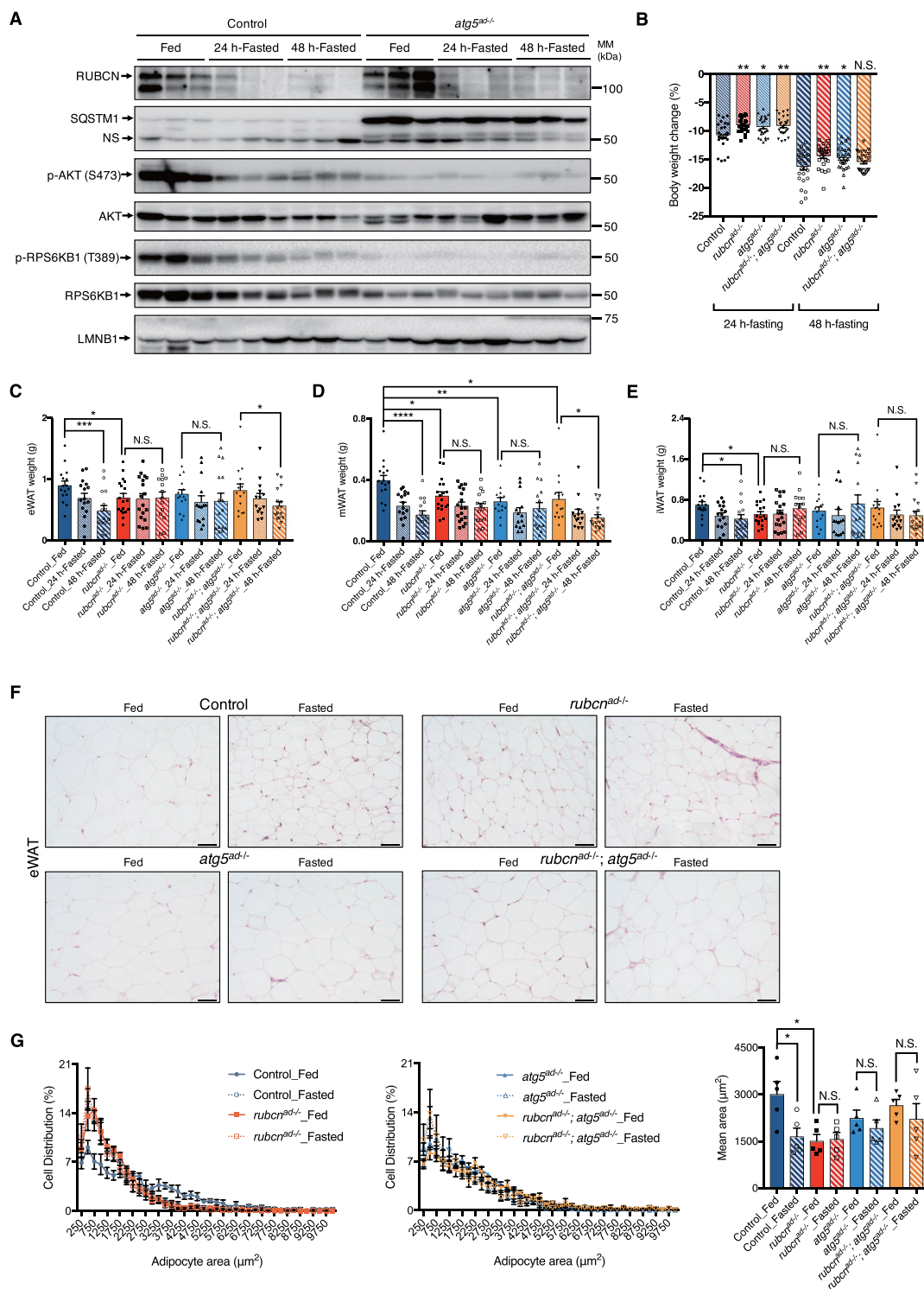
Figure 1. Loss of *atg5* in adipocytes mitigates the fasting-induced fat loss. (A) Immunoblotting to detect the indicated proteins in the eWAT depots of fed and 24- or 48-h-fasted mice of the indicated genotypes (n = 3). (B) Bodyweight ratio of mice of the indicated genotypes during fasting (n = 25–26). Data were analyzed using one-way ANOVA followed by Dunnett's test. (C) eWAT weight, (D) mWAT weight, and (E) iWAT weight of fed and 24- or 48-h-fasted mice of the indicated genotypes (n = 14–18). Data were analyzed using a two-tailed Student's *t*-test. (F) Representative images of H&E staining of eWAT sections from fed or 24-h-fasted mice of the indicated genotypes. Scale bars: 50 μm. (G) Distribution of adipocyte size in eWAT sections from fed or 24-h-fasted mice of the indicated genotypes in (F) (n = 5). Data were analyzed using a two-tailed Student's *t*-test. Quantification of the mean adipocyte area is shown in the graphs at the right. All data are presented as means ± SEM. *P < 0.05, **P < 0.01, ***P < 0.001, ****P < 0.0001, and N.S., not significant.

NCOA2 levels were reduced in the cytoplasmic fraction, but not in the nuclear fraction, during starvation (Figure 3G). Our previous study identified the mutant NCOA1 and NCOA2 that are resistant to autophagic degradation due to loss of

interaction with GABARAP family proteins [23]. We found that overexpression of the mutant NCOA1 and NCOA2 restored the starvation-induced reduction in the mRNA levels of adipogenic genes in 3T3-L1 adipocytes (Figure 3H). These
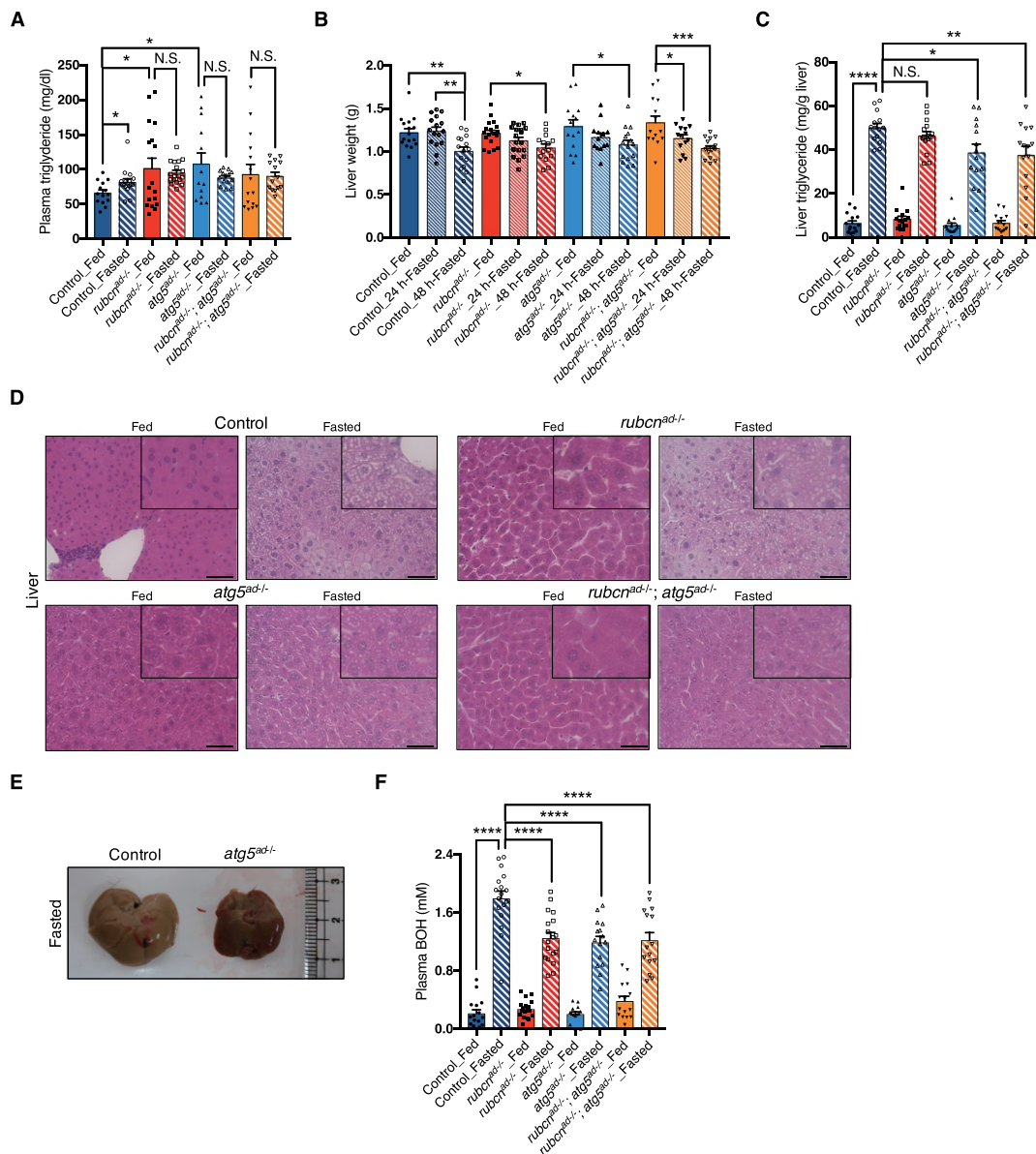
Figure 2. Loss of *atg5* in adipocytes reduces hepatic steatosis induced by fasting. (A) Plasma triglyceride levels in fed or 24-h-fasted mice of the indicated genotypes (n = 14–18). Data were analyzed using a two-tailed Student's *t*-test. (B) Liver weight of fed and 24- or 48-h-fasted mice of the indicated genotypes (n = 14–18). Data were analyzed using a two-tailed Student's *t*-test. (C) Liver triglyceride levels in fed or 24-h-fasted mice of the indicated genotypes (n = 15, 16). Data were analyzed using one-way ANOVA followed by Dunnett's test. (D) Representative images of H&E staining of liver sections from fed or 24-h-fasted mice of the indicated genotypes. Scale bars: 50 μm. (E) Representative images of the liver from 24-h-fasted mice of the indicated genotypes. (F) Plasma beta-hydroxybutyrate (BOH) levels in fed or 24-h-fasted mice of the indicated genotypes (n = 14–18). Data were analyzed using one-way ANOVA followed by Dunnett's test. All data are presented as means ± SEM. *P < 0.05, **P < 0.01, ***P < 0.001, and N.S., not significant.

data suggest that NCOA1 and NCOA2 in adipocytes are degraded by autophagy during starvation, and their reductions lead to a decrease in adipogenesis. This mechanism would account for the autophagy-dependent impairment of fasting-induced fat loss, hepatic steatosis, and ketonemia in *atg5* knockout mice.

A previous report showed that PNPLA2-dependent lipolysis largely contributes to the metabolic response to fasting [8]. Therefore, we sought to examine whether *rubcn* knockout or *atg5* knockout impairs lipolysis during fasting. LIPE is the rate-limiting enzyme in lipolysis and is activated via PRKA-mediated phosphorylation of S660 [27,28]. As well as control mice, both *rubcn*^ad−/−^ mice and *atg5*^ad−/−^ mice exhibited fasting-induced phosphorylation of S660 in LIPE (Figure S3E–G).

Moreover, control mice, *rubcn*^ad−/−^ mice, *atg5*^ad−/−^ mice, and the double knockout mice exhibited a fasting-induced increase in plasma epinephrine (Figure S3H), which stimulates PRKA activity [27,28]. *rubcn* knockout or *atg5* knockout did not reduce plasma levels of glycerol, a product of lipolysis (Figure S3I). Consistent with this, our previous study showed that loss of adipose *rubcn* does not affect *ex vivo* lipolysis or fasting-induced increase of plasma fatty acids [23]. Hepatic mRNA levels of *Cd36* and *Slc27a2/Fatp2*, which are fatty acid transporters, in fasted *rubcn*^ad−/−^ mice or *atg5*^ad−/−^ mice were comparable to those in fasted control mice (Figure S3J, 3K). These results suggest that *rubcn* knockout or *atg5* knockout does not impair lipolysis in adipocytes and subsequent fatty acid uptake in the liver. In addition, in fasting conditions, *rubcn* knockout
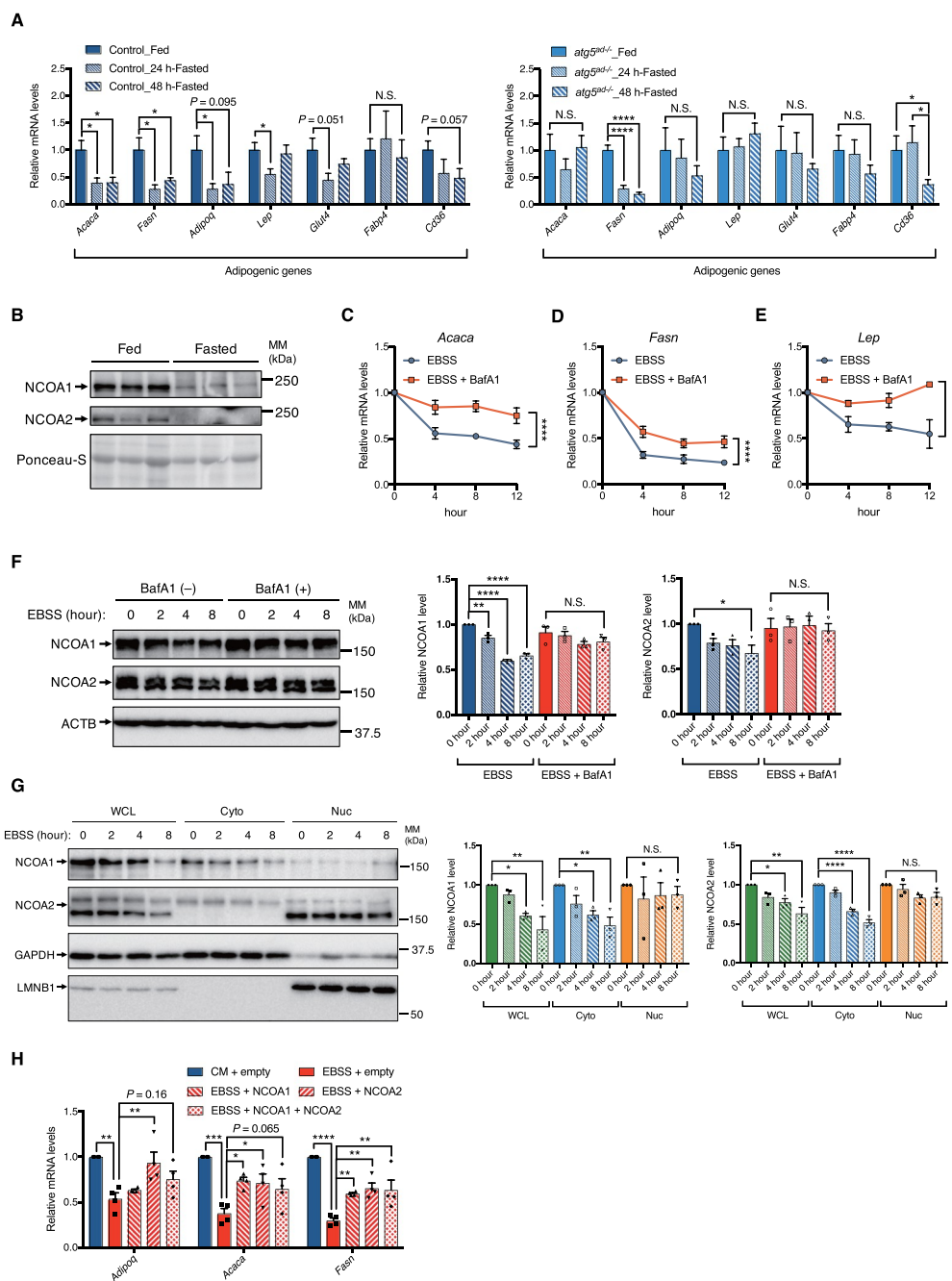
Figure 3. Adipose NCOA1 and NCOA2 levels are significantly reduced under starvation conditions. (A) Relative mRNA levels of the indicated genes in the eWAT depots of fed and 24- or 48-h-fasted mice of the indicated genotypes (n = 6). Data were analyzed using a two-tailed Student's t-test. (B) Immunoblotting to detect the indicated proteins in the eWAT depots of fed or 48-h-fasted wild-type mice (n = 3). (C–E) Relative mRNA levels on day 10 of the indicated genes in 3T3-L1 cells that were starved and cultured with or without 125 nM Baf A1 for the indicated times (n = 4). Data were analyzed using two-way ANOVA followed by Fisher's LSD test. (F) Immunoblotting to detect the indicated proteins on day 10 in 3T3-L1 cells that were starved and cultured with or without 125 nM Baf A1 for the indicated times (n = 3). Data were analyzed using one-way ANOVA followed by Dunnett's test. (G) Immunoblotting to detect the indicated proteins in the nuclear and cytoplasmic fractions of 3T3-L1 cells that were starved for the indicated times (n = 3). Data were analyzed using one-way ANOVA followed by Dunnett's test. (H) Relative mRNA levels of adipogenic genes in 3T3-L1 cells that were cultured in CM (Complete medium) or EBSS for 8 h. FLAG-W288A-NCOA1 and/or FLAG-W296A-NCOA2 plasmids were transfected for 24 h starting on day 9. The FLAG-only plasmid was used as an empty vector. Cells were harvested on day 10 (n = 4). Quantification of all data is shown on the graphs to the right of each blot. All data are presented as means ± SEM. *P < 0.05, **P < 0.01, ***P < 0.001, ****P < 0.0001, and N.S., not significant.

or *atg5* knockout did not decrease hepatic mRNA levels of *Dgat1* and *Gk*, which participate in *de novo* lipogenesis (Figure S3L, 3M). Previous studies showed that adipose lipolysis and hepatic lipogenesis significantly contribute to hepatic

steatosis [8,29]. Collectively, *de novo* lipogenesis and fatty acid uptake could contribute to the hepatic steatosis still seen in fasted *rubcn*[ad−/−] mice or *atg5*[ad−/−] mice (Figure 2C ,D). Fed *rubcn* knockout mice showed a fat loss (Figure 1C–E) and

increased plasma triglycerides (Figure 2A), but not robust hepatic steatosis that is observed in fasted mice (Figure 2C, D). It would be since lipid transport or lipogenesis in the liver is not activated in fed conditions (Figure S3J–M).

RUBCN is degraded by autophagy during starvation

One remaining question is: What is the mechanism by which RUBCN is downregulated in adipocytes during fasting? Surprisingly, we found that bafilomycin A1 treatment prevented

a starvation-induced reduction in RUBCN protein levels in 3T3-L1 adipocytes (Figure 4A). Also, in mouse adipose tissue, RUBCN protein levels were increased in an *ex vivo* culture model after treatment with lysosomal inhibitors (Figure 4B). Notably, bafilomycin A1 treatment also increased the levels of RUBCN in HeLa cells (Figure 4C), HEK293T cells (Figure S4A), and MEFs (Figure S4B). Furthermore, immunocytochemistry revealed that bafilomycin A$_1$ significantly increased the colocalization of GFP-RUBCN with MAP1LC3, which is an autophagosome marker (Figure 4D). These data indicate that RUBCN is
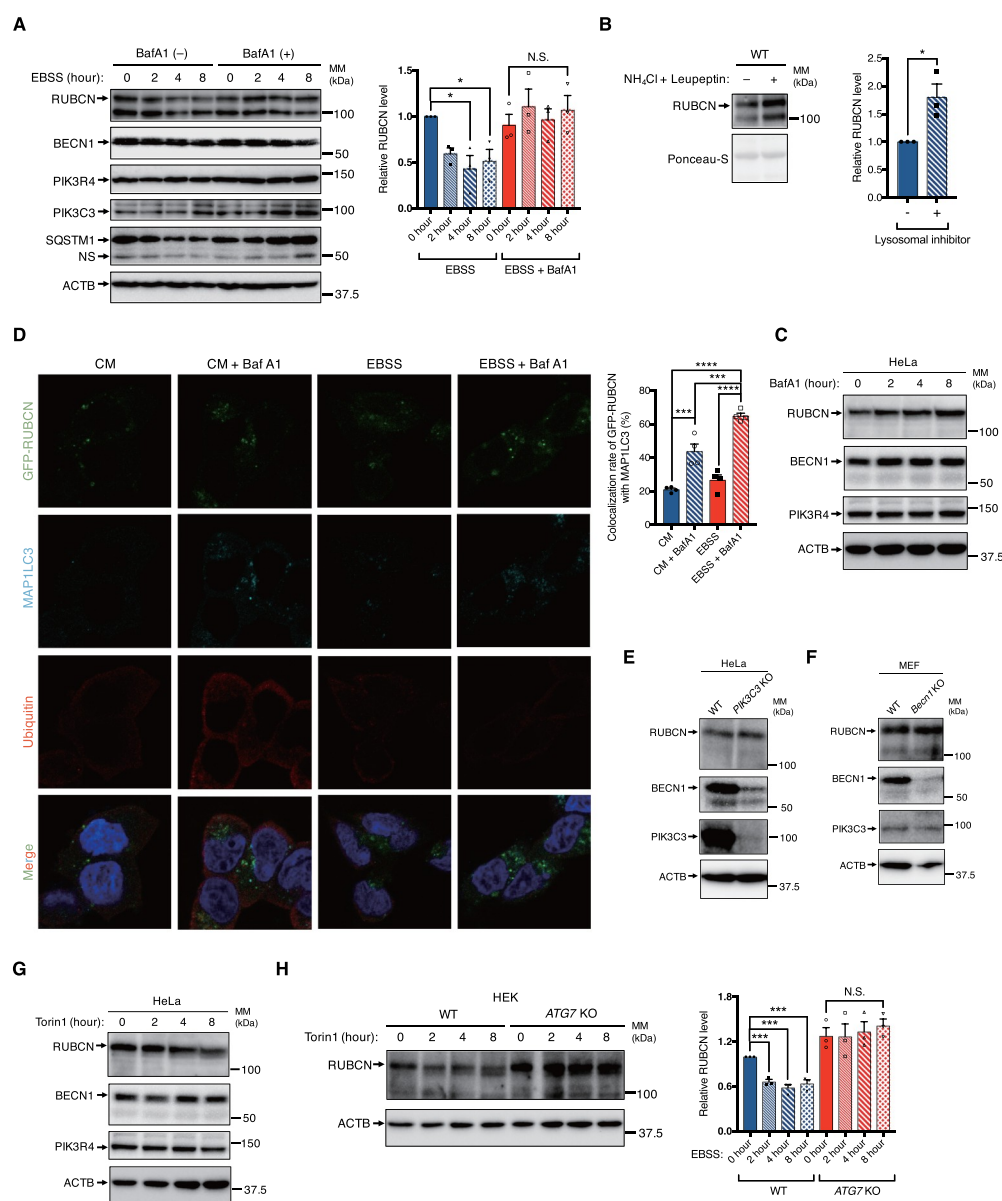

Figure 4. RUBCN is significantly decreased in an autophagy-dependent manner during fasting. (A) Immunoblotting to detect the indicated proteins on day 10 in 3T3-L1 cells that were starved and cultured with or without 125 nM Baf A1 for the indicated times (n = 3). Data were analyzed using one-way ANOVA followed by Dunnett's test. (B) Immunoblotting to detect the indicated proteins in wild-type eWAT depots explanted in DMEM, treated with or without 20 mM ammonium chloride and 200 μM leupeptin for 2 h (n = 3). Data were analyzed using a two-tailed Student's t-test. (C) Immunoblotting to detect the indicated proteins in HeLa cells that were treated with 125 nM Baf A1 for the indicated times. (D) Representative immunocytochemistry images to detect MAP1LC3 and Ubiquitin in HEK293T cells stably expressing GFP-RUBCN. Cells were cultured in CM or EBSS with or without 125 nM Baf A1 for 8 h. Scale bars: 30 μm (n = 4). (E) Immunoblotting to detect the indicated proteins in wild-type or *PIK3C3* knockout HeLa cells. (F) Immunoblotting to detect the indicated proteins in wild-type or *Becn1* knockout MEFs. (G) Immunoblotting to detect the indicated proteins in HeLa cells that were treated with 250 nM Torin-1 for the indicated times. (H) Immunoblotting to detect the indicated proteins in wild-type or *ATG7* knockout HEK293T cells that were treated with 250 nM Torin-1 for the indicated times (n = 3). Data were analyzed using one-way ANOVA followed by Dunnett's test. Quantification of the data is shown on the graphs to the right of each blot. All data are presented as means ± SEM. *P < 0.05, **P < 0.01, ***P < 0.001, ****P < 0.0001, and N.S., not significant.

internalized in autophagosomes and is degraded in lysosomes in adipocytes and other cell types.

RUBCN negatively regulates autophagy by interacting with the autophagic PtdIns3K complex [21,22]. The protein levels of other components of the PtdIns3K complex, such as PIK3R4/VPS15, PIK3C3/VPS34, and BECN1/Beclin 1, did not change under starvation conditions or after bafilomycin A$_1$ treatment (Figure 4A,C). Therefore, we investigated whether RUBCN is stable when the PtdIns3K complex is disrupted. Disruption of the PtdIns3K complex by knockout of *PIK3C3* (Figure 4E) or *Becn1* (Figure 4F) did not affect the levels of RUBCN, suggesting that RUBCN could be degraded independent from the PtdIns3K complex.

Notably, upon fasting, phosphorylation of AKT and RPS6KB1 was significantly reduced in mouse adipose tissue (Figure 1A) and 3T3-L1 adipocytes (Figure S4C), suggesting that the AKT-MTORC1 pathway is downregulated during fasting. Because MTORC1 negatively regulates autophagy [25], we investigated whether MTORC1 regulates the protein levels of RUBCN and found that an MTORC1 inhibitor significantly reduced the levels of RUBCN in HeLa cells (Figure 4G), HEK293T cells (Figure S4D), and MEFs (Figure S4E). In contrast, *rubcn* knockout did not affect the fasting-induced reduction in phosphorylation of AKT and RPS6KB1 (Figure S4F). Furthermore, knockout of *ATG7*, an essential gene for autophagy, abolished the reduction of RUBCN protein levels observed after MTORC1 inhibitor treatment (Figure 4H), suggesting that RUBCN is degraded by autophagy upon downregulation of MTORC1 during starvation. Because RUBCN negatively regulates autophagy, it is conceivable that the degradation of RUBCN mediates the negative regulation of autophagy by the MTORC1 pathway. On the other hand, RUBCN was accumulated in $atg5^{ad-/-}$ mice but was decreased during fasting (Figure 1A), suggesting that other mechanisms also contribute to the fasting-induced reduction of adipose RUBCN. Because mRNA levels of adipose *Rubcn* tended to decrease in $atg5^{ad-/-}$ mice (Figure S4G), transcriptional regulation would be one of the mechanisms. In addition, our previous study showed that RUBCN could be degraded by proteasome [30]; therefore, the proteasome pathway could also be one of the mechanisms.

To further examine how autophagy degrades RUBCN protein, we tested the requirement of Atg8-family proteins (MAP1LC3A, MAP1LC3B, MAP1LC3C, GABARAP, GABARAPL1, and GABARAPL2) on the degradation of RUBCN during starvation. Starvation induced a reduction in levels of RUBCN in the Hexa knockout HeLa cells (Figure S4H) that lack all of the Atg8-family proteins proteins [31], suggesting that Atg8-family proteins are dispensable for the degradation of RUBCN. Consistent with this, FLAG-RUBCN did not interact with either of the Atg8-family proteins (Figure S4J). We also used the Penta knockout HeLa cells that lack autophagy receptors (CALCOCO2/NDP52, OPTN [optineurin], TAX1BP1, SQSTM1, and NBR1) [32]. RUBCN did not decrease in starvation in the Penta knockout HeLa cells (Figure S4I); however, RUBCN did not interact with either of the autophagy receptors (Figure S4K). In addition, GFP-RUBCN did not colocalize with ubiquitin (Figure 4D). Because autophagy receptors bind to their substrates via ubiquitination, it is conceivable that autophagy

receptors are not a direct contributor to the degradation of RUBCN. Taken together, we conclude that RUBCN is degraded by autophagy, resulting in a decrease in RUBCN protein levels during fasting.

Discussion

Lipids stored in adipocytes are transferred into the liver during fasting [7], and the hepatic lipids are used for various metabolic processes, including ketogenesis [6]. PNPLA2-mediated lipolysis in adipocytes is a major contributor to the metabolic response to nutrient deprivation, including fat atrophy, hepatic steatosis, and ketonemia [8]. However, it remains unknown whether other pathways in adipocytes contribute to the fasting response. This study suggests that increased autophagic activity mediates a reduction in adipogenesis during fasting, leading to hepatic steatosis and ketogenesis. Indeed, loss of *atg5* in adipocytes attenuated, but did not eliminate, systemic fat loss (Figure 1), hepatic steatosis, or ketonemia (Figure 2). These phenotypes were similar to but weaker than those observed in the *pnpla2* knockout mice [8]. In addition, our present study suggests that RUBCN or ATG5 is not involved in lipolysis in adipocytes (Figure S3). Therefore, it is possible that an autophagy-mediated reduction in adipogenesis plays a role in the lipolysis-independent response to fasting.

In a previous study, we demonstrated that aging leads to a substantial decrease in adipose RUBCN, the loss of which promotes age-associated metabolic disorders through increased autophagic activity [23]. Our present findings show that fasting also reduces adipose levels of RUBCN, and elevated autophagy promotes a metabolic response to fasting, which phenocopies the metabolic disorders in aging. Namely, age-associated metabolic disorders share mechanisms with the fasting response in adipocytes. The remaining mechanistic link to be elucidated is how adipose RUBCN is reduced and autophagic activity is increased during fasting or aging. In this regard, the findings of this study revealed that RUBCN is degraded by autophagy in adipocytes (Figure 4). Adipose *Rubcn* mRNA levels are also significantly reduced in aging mice [23]. MTORC1 activity in adipocytes is downregulated during aging [33] and fasting [34]. Therefore, upregulation of autophagy in adipocytes could be initiated in aging and fasting via inhibition of MTORC1 and transcriptional regulation of *Rubcn*. Because MTORC1 regulates other metabolic pathways in addition to autophagy [35], adipose-specific knockout mice of *mtor* or *rptor* develop more severe hepatic steatosis than *rubcn* knockout mice in fed conditions [36,37]. The regulator of MTORC1 activity in adipocytes during aging is of particular interest in the field of metabolism. Moreover, previous studies revealed that MTORC1 directly phosphorylates and inhibits an autophagy initiator ULK1; in turn, inhibition of MTORC1 promotes autophagosome formation [38]. In contrast, RUBCN binds to and inhibits the PtdIns3K complex that is crucial for autophagosome maturation [22]; therefore, it is conceivable that inhibition of MTORC1 initiates autophagy and promotes the degradation of RUBCN, thereby enhancing autophagosome maturation further. Future studies will hopefully determine

the specific process by which RUBCN is degraded by autophagy.

In summary, we discovered that RUBCN mediates upregulation of autophagy in adipocytes during fasting and that elevated adipose autophagy contributes to fasting-induced metabolic responses, including systemic fat loss, hepatic steatosis, and ketonemia. These results provide novel insight into adipose autophagy, which plays a pivotal role in age-associated metabolic disorders.

Materials and methods

Reagents and antibodies

The following antibodies were used for western blotting at the indicated dilutions: rabbit monoclonal anti-RUBCN/rubicon (Cell Signaling Technology [CST], 8465; 1:1000), rabbit polyclonal anti-ATG12 (CST, 2011; 1:2000), rabbit polyclonal anti-PIK3C3/VPS34 [22] (1:3000), mouse monoclonal anti-PIK3R4/VPS15 (Abnova, H00030849-M03; 1:2000), mouse monoclonal anti-BECN1/Beclin 1 (BD, 612,112; 1:2000), rabbit polyclonal anti-MAP1LC3 (MBL, PM036; 1:2000), rabbit monoclonal anti-MAP1LC3A (CST, 4599; 1:2000), rabbit polyclonal anti-MAP1LC3A/B (CST, 4108; 1:2000), rabbit monoclonal anti-MAP1LC3C (CST, 14,736; 1:2000), rabbit polyclonal anti-GABARAP (MBL, PM037; 1:2000), rabbit polyclonal anti-GABARAPL1 (abcam, ab86497; 1:2000), rabbit polyclonal anti-GABARAPL2 (MBL, PM038, 1:2000), rabbit polyclonal anti-SQSTM1/p62 (MBL, PM045; 1:5000), rabbit monoclonal anti-TAX1BP1 (CST, 5105, 1:2000), rabbit monoclonal anti-NBR1 (CST, 9891; 1:2000), rabbit monoclonal anti-OPTN/optineurin (CST, 58,981; 1:2000), rabbit monoclonal anti-CALCOCO2/NDP52 (CST, 60,732; 1:2000), rabbit polyclonal anti-ULK1 (Santa Cruz Biotechnology, sc-33,182; 1:2000), rabbit polyclonal anti-phospho-ULK1 (S757; CST, 6888; 1:2000), rabbit polyclonal anti-RPS6KB1/S6K1 (CST, 9202; 1:2000), rabbit polyclonal anti-phospho-RPS6KB1/S6K1 (T389; CST, 9205; 1:2000), rabbit polyclonal anti-AKT (CST, 9272; 1:2000), rabbit polyclonal anti-phospho-AKT (S473; CST, 9271; 1:2000), rabbit polyclonal anti-LIPE/HSL (CST, 4107; 1:2000), rabbit polyclonal anti-phospho-LIPE/HSL (S660) (CST, 45,804; 1:2000), rat monoclonal anti-ADIPOQ/adiponectin (R&D Systems, MAB1119; 1:2000), mouse monoclonal anti-FABP4 (Santa Cruz Biotechnology, sc-271,529; 1:2000), mouse monoclonal anti-PPARG (Santa Cruz Biotechnology, sc-7273; 1:2000), rabbit monoclonal anti-NCOA1/SRC-1 (CST, 2191; 1:2000), rabbit polyclonal anti-NCOA2/TIF2 (Bethyl Laboratories, A300-346A; 1:2000), mouse monoclonal antiTUBA4A/α-tubulin (Sigma-Aldrich, T5168; 1:25,000), mouse monoclonal anti-ACTB/β-actin (MBL, M177-3; 1:25,000), rabbit monoclonal anti-GAPDH (CST, 2118; 1:25,000), goat monoclonal anti-LMNB1/lamin B1 (Santa Cruz Biotechnology, sc-6217; 1/1000), HRP-conjugated goat anti–rabbit IgG (Jackson ImmunoResearch, 111–035-003; 1:2000), HRP-conjugated goat anti-rat IgG (Jackson ImmunoResearch, 112–035-003; 1:2000), and HRP-conjugated goat anti–mouse IgG (Jackson ImmunoResearch, 115–035-003; 1:2000). The following antibodies were used for immunocytochemistry at the indicated dilution: rabbit polyclonal anti-MAP1LC3 (MBL, PM036;

1:2000), mouse monoclonal anti-Ubiquitin (Nippon Bio-test laboratories, 0918–2; 1:10,000), Alexa Fluor 488 goat anti-mouse IgG (Abcam, ab150117; 1:500), and Alexa Fluor 647 goat anti-rabbit IgG (Invitrogen, A27040; 1:500). Bafilomycin A$_1$ and Torin-1 were purchased from Cayman Chemical (11,038) and Tocris (4247), respectively.

Animals

C57BL/6 J mice were obtained from the CLEA Japan (C57BL/6 JJcl). *Adipoq-Cre* mice [39], *rubcn*-floxed mice [30,40], *atg5*-floxed mice [10], *rubcn*$^{ad-/-}$ mice, *atg5*$^{ad-/-}$ mice, and *rubcn*$^{ad-/-}$; *atg5*$^{ad-/-}$ mice in the C57BL/6J background were used in this study. All mice used were not littermates because we used *Adipoq-Cre* mice as controls to exclude the possibility that the phenotypes of the knockout mice arose from *Cre*-recombinase–mediated cellular dysfunction [41]. The following primer sets were used for genotyping by PCR: 5…-ACAACGACAATCACACAGAC-3… and 5…-TGACGAGGGG TAATGGATAG-3… for *rubcn* wild-type and floxed allele; 5…-ACAACGACAATCACACAGAC-3… and 5…-AATCCTTCGCC CCTTTTACC-3… for *rubcn* deleted allele; 5…-GAATATG AAGGCACACCCCTGAAATG-3…, 5…-GACAGGTCGGTCTT GACAAAAAGAAC-3… and 5…-GTACTGCATAATGGTTTA ACTCTTGC-3… for *atg5* wild-type and floxed allele; 5…-GCTCTTAGTCCAGAACCTAAACC-3… and 5…-GTACT GCATAATGGTTTAACTCTTGC-3… for *atg5* deleted allele; and 5…-GCATTACCGGTCGATGCAACGAGTGATGAG-3… and 5…-GAGTGAACGAACCTGGTCGAAATCAGTGCG-3… for *Cre*. All mice used were 5- to 6-month-old males. These mice were maintained on an NCD with 12-h light/12-h dark cycles. The ambient temperature and humidity were 23°C ± 1.5°C and 45% ± 15%, respectively. Food and water were provided *ad libitum*. The following kits were used to measure metabolic parameters: a triglyceride determination kit (Wako, 432–40,201), a glycerol standard solution (Sigma-Aldrich, G7793), a free glycerol reagent (Sigma-Aldrich, F6428), a Ketone Body Assay Kit (EnzyChrom, EKBD-100), and an epinephrine ELISA kit (BioVision, B4359). The Institutional Committee of Osaka University approved experimental procedures using mice.

Cell culture and plasmid transfection

3T3-L1 cells were purchased from the National Institute of Biomedical Innovation, JCRB Cell Bank (JCRB9014). HeLa Kyoto cells were previously used in our laboratory [42]. *becn1* KO MEFs and *ATG7* KO HEK293T cells were a kind gift from Dr. Shizuo Akira (Osaka University) and Dr. Masaaki Komatsu (Juntendo University), respectively. The Hexa (Atg8-family proteins) knockout HeLa cells [31] and the Penta (Autophagy receptors) knockout HeLa cells [32] were gifted by Dr. Michael Lazarou (Monash University). Cells were cultured in Dulbecco's Modified Eagle's Medium (DMEM; Sigma-Aldrich, D6429) with 10% fetal bovine serum (FBS) and 1% penicillin–streptomycin (Sigma-Aldrich, P4333) at 37°C with 5% CO$_2$. Two days post-confluence (defined as day 0), 3T3-L1 cells were treated for 48 h with an adipogenic cocktail containing 0.5 mM 3-isobutyl-

1-methylxanthine (Nacalai Tesque, 19,624–86), 1 μM dexamethasone (Sigma-Aldrich, D1756), 1 μM insulin (Nacalai Tesque, 19,252–24), and 10 μM pioglitazone (Wako, 162–24,831) to induce adipogenesis. After that, the medium was replaced with DMEM with 10% FBS. According to the manufacturer's protocol, plasmid transfection was carried out using Opti-MEM (Gibco, 31,985,062) and Lipofectamine 2000 (Invitrogen, 11,668,027). Earle's Balanced Salts (EBSS; Sigma-Aldrich, E2888) was used for starvation treatment. The cells were routinely tested for mycoplasma infection and confirmed as negative for mycoplasma contamination.

Plasmids

pcDNA3.1 were purchased from Invitrogen (V79020). pMRX-IRES-bsr was kindly gifted from Dr. Shoji Yamaoka (Tokyo Medical and Dental University, Tokyo, Japan). pcDNA3.1–3xFLAG-W288A-mouseNCOA1 (mNCOA1) and pcDNA3.1-FLAG-W296A-mNCOA2 were previously generated [23]. pcDNA3.1-FLAG-humanRUBCN (HsRUBCN) was generated from pcDNA3.1 and pGAD-hRUBCN [43]. pMRX-bsr-GFP-mRUBCN was generated from pMRX-IRES-bsr and GFP-mRUBCN [22]. Retroviruses were prepared as previously described [44]. Stable transformants were selected with 5 μg/ml blasticidin.

CRISPR Cas9 system

ATG34 KO HeLa cells were generated using a CRISPR-Cas9 system. Annealed gRNA oligonucleotides were inserted into the px458 vector (Addgene, 48,138; deposited by Feng Zhang), and the gRNA construct was transfected into HeLa cells using the transfection reagent ViaFect (Promega, E4981). GFP-positive single cells were sorted into 96-well plates using FACS. Candidate single-clone colonies were verified by immunoblotting using specific antibodies, an autophagy flux assay, and genomic DNA sequencing. The gRNA sequences were as follows: 5…-CTACATCTATAGTTGTGACC-3…

Immunocytochemistry

Cells were fixed with 4% PFA in PBS (Santa Cruz Biotechnology, sc-281,692) for 20 min at room temperature and permeabilized with 50 μg/ml digitonin (Sigma-Aldrich, D141) in PBS for 10 min at room temperature. The cells were washed with PBS once and blocked with 0.2% gelatin (Sigma-Aldrich, G9391) in PBS for 30 min at room temperature. Next, the cells were incubated with the primary antibody in 0.2% gelatin in PBS for 60 min at room temperature. After being washed with PBS twice, the cells were incubated with the secondary antibody in 0.2% gelatin in PBS for 60 min at room temperature. After being washed with PBS twice, the coverslips were mounted onto slides using VECTASHIELD® PLUS Antifade Mounting Medium with DAPI (Vector Laboratories, H-1900). Images were acquired on an LSM 880 confocal microscope (Zeiss).

Histological analyses

Tissues were fixed in 4% paraformaldehyde overnight and stored in 70% ethanol until processing. Tissues were paraffinized and sectioned at 5 μm by microtome (Leica). The slides were stained with H&E according to a standard protocol [45]. Images were acquired on a BZ-X700 microscope (Keyence). Adipocyte size was measured on a BZ-X700 microscope.

Liver TG content

Liver samples (50 mg) were homogenized in 1 mL of Folch solution (2:1 v:v chloroform:methanol) using a Precellys Evolution tissue homogenizer (Bertin, P000062-PEVO0-A), and 200 μL of a 0.9% NaCl solution was added to the homogenates. The lower phase was collected, and TG content was measured using the triglyceride determination kit (Wako, 432–40,201).

RNA isolation and quantitative PCR analyses

Mouse tissues were harvested in QIAzol (Qiagen, 79,306) using a Precellys Evolution tissue homogenizer. Total RNA was extracted using the RNeasy Plus Mini kit (Qiagen, 74,134). cDNA was generated using iScript (Bio-Rad, 1,708,891). qRT-PCR was performed with *Power* SYBR Green (Applied Biosystems, 4,367,659) on a QuantStudio 7 Flex Real-time PCR System (Applied Biosystems). Four technical replicates were performed for each reaction. *36b4* was used as an internal control for adipose tissue and 3T3-L1 adipocytes. *Gusb* was used as an internal control for the liver. The sequences of the qRT-PCR primers are shown in Table S1.

Immunoblotting

Mouse tissues were harvested in RIPA buffer (50 mM Tris-HCl, pH 8.0, 150 mM NaCl, 1% w:v Triton X-100 [Nacalai Tesque, 35,501–15], 0.1% SDS, 0.5% sodium deoxycholate [Sigma Aldrich, D6750], and protease inhibitor cocktail [Roche, 11,873,580,001]) using a Precellys Evolution tissue homogenizer, and cells were lysed in the same buffer. After centrifugation at 20,380 x g for 5 min, the protein concentration in the supernatants was measured using a BCA assay (Nacalai Tesque, 06385–00). Lysates were mixed with 5× SDS sample buffer and boiled for 5 min. Protein lysates were separated by 7% or 13% SDS-PAGE and transferred to PVDF membranes. Membranes were stained with Ponceau-S, blocked with 1% skim milk TBS-T, and incubated with the indicated primary antibodies. Immunoreactive bands were detected using HRP-conjugated secondary antibodies, visualized with Luminata Forte (Merck Millipore, 61–0206-81) or ImmunoStar LD (Wako, 290–69,904), and imaged using a ChemiDoc Touch (Bio-Rad) imager. TUBA4A/α-tubulin, ACTB/β-actin, GAPDH, and LMNB1 were used as loading controls. The band intensity of each protein was normalized against the loading control for quantification. Band intensity was quantified using the ImageJ software (NIH).

Immunoprecipitation assay

Cells were lysed with lysis buffer (50 mM Tris-HCl, pH 7.4, 150 mM NaCl, 10% [w:v] glycerol [Fisher Scientific, G33-1], 1% Triton X-100, Complete protease inhibitor cocktail [Roche, 11,873,580,001]). After centrifugation at 21,300 x g for 5 min, the resultant supernatants were quantified by a BCA assay. The samples were incubated overnight at 4°C with anti-FLAG M2 affinity gel (Sigma-Aldrich, A2220). After repeated washing with wash buffer (50 mM Tris-HCl, pH 7.4, 150 mM NaCl, 0.1% Triton X-100), the bound proteins were eluted with SDS sample buffer and were analyzed by SDS–PAGE and immunoblotting.

Ex vivo culture assay

Freshly collected tissue explants were incubated for 2 h in high-glucose DMEM with or without 20 mM ammonium chloride and 200 μM leupeptin (Peptide Institute, 4041) at 37°C with 5% CO_2 [20]. Explants were processed and immunoblotted for RUBCN.

Nuclear/cytoplasmic fractionation assay

Cells were lysed with 0.1% NP-40 (Nacalai Tesque, 25,223–75) and protease inhibitor cocktail in PBS. An aliquot of each lysate was mixed with 5× SDS sample buffer and used as a whole-cell lysate. Another aliquot was centrifuged at 20,380 x g for 5 min; the resultant supernatant was mixed with 5× SDS sample buffer and used as the cytoplasmic fraction. The pellet was washed once, lysed in SDS sample buffer, and used as the nuclear fraction.

Statistical analyses

All results are presented as means ± SEM. Statistical analysis was performed with two-tailed Student's t-test, one-way ANOVA followed by Tukey's test or Dunnett's test, or two-way ANOVA followed by Fisher's LSD test using Excel for Mac (Microsoft) and GraphPad Prism7 (GraphPad Software).

Acknowledgments

Disclosure statement

Funding

Data availability

All data are also available from the corresponding author upon reasonable request.

ORCID

Tadashi Yamamuro 🄳 http://orcid.org/0000-0002-0610-5204
Shuhei Nakamura 🄳 http://orcid.org/0000-0002-1488-8317
Kyosuke Yanagawa 🄳 http://orcid.org/0000-0002-9645-5899
Tsuyoshi Kawabata 🄳 http://orcid.org/0000-0003-0899-0750
Atsunori Fukuhara 🄳 http://orcid.org/0000-0002-6289-3778
Tamotsu Yoshimori 🄳 http://orcid.org/0000-0001-9787-3788

References

[1] Kahn CR, Wang G, Lee KY. Altered adipose tissue and adipocyte function in the pathogenesis of metabolic syndrome. J Clin Invest. 2019;129:3990–4000.

[2] Olzmann JA, Carvalho P. Dynamics and functions of lipid droplets. Nat Rev Mol Cell Bio. 2019;20:137–155.

[3] Matsuzawa Y. The metabolic syndrome and adipocytokines. Febs Lett. 2006;580:2917–2921.

[4] Ahima RS, Flier JS. Adipose tissue as an endocrine organ. Trends Endocrinol Metab. 2000;11:327–332.

[5] Reinisch I, Schreiber R, Prokesch A. Regulation of thermogenic adipocytes during fasting and cold. Mol Cell Endocrinol. 2020;512:110869.

[6] Puchalska P, Crawford PA. Multi-dimensional roles of ketone bodies in fuel metabolism, signaling, and therapeutics. Cell Metab. 2017;25:262–284.

[7] Geisler CE, Renquist BJ. Hepatic lipid accumulation: cause and consequence of dysregulated glucoregulatory hormones. J Endocrinol. 2017;234:R1–21.

[8] Wu JW, Wang SP, Casavant S, et al. Fasting energy homeostasis in mice with adipose deficiency of desnutrin/adipose triglyceride lipase. Endocrinology. 2012;153:2198–2207.

[9] Komatsu M, Waguri S, Chiba T, et al. Loss of autophagy in the central nervous system causes neurodegeneration in mice. Nature. 2006;441:880–884.

[10] Hara T, Nakamura K, Matsui M, et al. Suppression of basal autophagy in neural cells causes neurodegenerative disease in mice. Nature. 2006;441:885–889.

[11] Komatsu M, Waguri S, Koike M, et al. Homeostatic levels of p62 control cytoplasmic inclusion body formation in autophagy-deficient mice. Cell. 2007;131:1149–1163.

[12] Komatsu M, Waguri S, Ueno T, et al. Impairment of starvation-induced and constitutive autophagy in Atg7-deficient mice. J Cell Biol. 2005;169:425–434.

[13] Masiero E, Agatea L, Mammucari C, et al. Autophagy is required to maintain muscle mass. Cell Metab. 2009;10:507–515.

[14] Nakai A, Yamaguchi O, Takeda T, et al. The role of autophagy in cardiomyocytes in the basal state and in response to hemodynamic stress. Nat Med. 2007;13:619–624.

[15] Zhang Y, Goldman S, Baerga R, et al. Adipose-specific deletion of autophagy-related gene 7 (atg7) in mice reveals a role in adipogenesis. Proc Natl Acad Sci. 2009;106:19860–19865.

[16] Singh R, Xiang Y, Wang Y, et al. Autophagy regulates adipose mass and differentiation in mice. J Clin Invest. 2009;119:3329–3339.

[17] Altshuler-Keylin S, Shinoda K, Hasegawa Y, et al. Beige adipocyte maintenance is regulated by autophagy-induced mitochondrial clearance. Cell Metab. 2016;24:402–419.

[18] Lu X, Altshuler-Keylin S, Wang Q, et al. Mitophagy controls beige adipocyte maintenance through a Parkin-dependent and UCP1-independent mechanism. Sci Signal. 2018;11:eaap8526.

[19] Martinez-Lopez N, Garcia-Macia M, Sahu S, et al. Autophagy in the CNS and periphery coordinate lipophagy and lipolysis in the brown adipose tissue and liver. Cell Metab. 2016;23:113–127.

[20] Martinez-Lopez N, Tarabra E, Toledo M, et al. System-wide benefits of intermeal fasting by autophagy. Cell Metab. 2017;26:856–871.e5.

[21] Zhong Y, Wang QJ, Li X, et al. Distinct regulation of autophagic activity by Atg14L and Rubicon associated with Beclin 1–phosphatidylinositol-3-kinase complex. Nat Cell Biol. 2009;11:468–476.

[22] Matsunaga K, Saitoh T, Tabata K, et al. Two Beclin 1-binding proteins, Atg14L and Rubicon, reciprocally regulate autophagy at different stages. Nat Cell Biol. 2009;11:385–396.

[23] Yamamuro T, Kawabata T, Fukuhara A, et al. Age-dependent loss of adipose Rubicon promotes metabolic disorders via excess autophagy. Nat Commun. 2020;11:4150.

[24] Picard F, Géhin M, Annicotte J-S, et al. SRC-1 and TIF2 control energy balance between white and brown adipose tissues. Cell. 2002;111:931–941.

[25] Lee PL, Jung SM, Guertin DA. The complex roles of mechanistic target of rapamycin in adipocytes and beyond. Trends Endocrinol Metab. 2017;28:319–339.

[26] Kawabata T, Yoshimori T. Autophagosome biogenesis and human health. Cell Discov. 2020;6:33.

[27] Kraemer FB, Shen W-J. Hormone-sensitive lipase. J Lipid Res. 2002;43:1585–1594.

[28] Duncan RE, Ahmadian M, Jaworski K, et al. Regulation of lipolysis in adipocytes. Nutrition. 2007;27:79–101.

[29] Kim C-W, Addy C, Kusunoki J, et al. Acetyl CoA carboxylase inhibition reduces hepatic steatosis but elevates plasma triglycerides in mice and humans: a bedside to bench investigation. Cell Metab. 2017;26:394–406.e6.

[30] Tanaka S, Hikita H, Tatsumi T, et al. Rubicon inhibits autophagy and accelerates hepatocyte apoptosis and lipid accumulation in nonalcoholic fatty liver disease in mice. Hepatology. 2016;64:1994–2014.

[31] Nguyen TN, Padman BS, Usher J, et al. Atg8 family LC3/GABARAP proteins are crucial for autophagosome–lysosome fusion but not autophagosome formation during PINK1/Parkin mitophagy and starvation. J Cell Biol. 2016;215:857–874.

[32] Lazarou M, Sliter DA, Kane LA, et al. The ubiquitin kinase PINK1 recruits autophagy receptors to induce mitophagy. Nature. 2015;524:309–314.

[33] Linford NJ, Beyer RP, Gollahon K, et al. Transcriptional response to aging and caloric restriction in heart and adipose tissue. Aging Cell. 2007;6:673–688.

[34] Ricoult SJH, Manning BD. The multifaceted role of mTORC1 in the control of lipid metabolism. Embo Rep. 2013;14:242–251.

[35] Laplante M, Sabatini DM. An emerging role of mTOR in lipid biosynthesis. Curr Biol. 2009;19:R1046–52.

[36] Shan T, Zhang P, Jiang Q, et al. Adipocyte-specific deletion of mTOR inhibits adipose tissue development and causes insulin resistance in mice. Diabetologia. 2016;59:1995–2004.

[37] Li Y, Chao X, Wang S, et al. Role of mechanistic target of rapamycin and autophagy in alcohol-induced adipose atrophy and liver injury. Am J Pathol. 2020;190:158–175.

[38] Kim J, Kundu M, Viollet B, et al. AMPK and mTOR regulate autophagy through direct phosphorylation of Ulk1. Nat Cell Biol. 2011;13:132–141.

[39] Eguchi J, Kong X, Tenta M, et al. Interferon regulatory factor 4 regulates obesity-induced inflammation through regulation of adipose tissue macrophage polarization. Diabetes. 2013;62:3394–3403.

[40] Yamamuro T, Nakamura S, Yamano Y, et al. Rubicon prevents autophagic degradation of GATA4 to promote Sertoli cell function. Plos Genet. 2021;17:e1009688.

[41] Loonstra A, Vooijs M, Beverloo HB, et al. Growth inhibition and DNA damage induced by Cre recombinase in mammalian cells. Proc Natl Acad Sci. 2001;98:9209–9214.

[42] Nakamura S, Shigeyama S, Minami S, et al. LC3 lipidation is essential for TFEB activation during the lysosomal damage response to kidney injury. Nat Cell Biol. 2020;22:1252–1263.

[43] Tabata K, Matsunaga K, Sakane A, et al. Rubicon and PLEKHM1 negatively regulate the endocytic/autophagic pathway via a novel Rab7-binding domain. Mol Biol Cell. 2010;21:4162–4172.

[44] Yoneshiro T, Wang Q, Tajima K, et al. BCAA catabolism in brown fat controls energy homeostasis through SLC25A44. Nature. 2019;572:614–619.

[45] Cardiff RD, Miller CH, Munn RJ. Manual hematoxylin and eosin staining of mouse tissue sections. Cold Spring Harb Protoc. 2014;2014:db.prot073411.